Metabolic modeling of the International Space Station microbiome reveals key microbial interactions

Rachita K. Kumar[1,2] , Nitin Kumar Singh[3] , Sanjaay Balakrishnan[2,4] , Ceth W. Parker[3] ,
Karthik Raman[1,2,4]* and Kasthuri Venkateswaran[3]*

Abstract

Background: Recent studies have provided insights into the persistence and succession of microbes aboard the International Space Station (ISS), notably the dominance of *Klebsiella pneumoniae*. However, the interactions between the various microbes aboard the ISS and how they shape the microbiome remain to be clearly understood. In this study, we apply a computational approach to predict possible metabolic interactions in the ISS microbiome and shed further light on its organization.

Results: Through a combination of a systems-based graph-theoretical approach, and a constraint-based community metabolic modeling approach, we demonstrated several key interactions in the ISS microbiome. These complementary approaches provided insights into the metabolic interactions and dependencies present amongst various microbes in a community, highlighting key interactions and keystone species. Our results showed that the presence of *K. pneumoniae* is beneficial to many other microorganisms it coexists with, notably those from the *Pantoea* genus. Species belonging to the *Enterobacteriaceae* family were often found to be the most beneficial for the survival of other microorganisms in the ISS microbiome. However, *K. pneumoniae* was found to exhibit parasitic and amensalistic interactions with *Aspergillus* and *Penicillium* species, respectively. To prove this metabolic prediction, *K. pneumoniae* and *Aspergillus fumigatus* were co-cultured under normal and simulated microgravity, where *K. pneumoniae* cells showed parasitic characteristics to the fungus. The electron micrography revealed that the presence of *K. pneumoniae* compromised the morphology of fungal conidia and degenerated its biofilm-forming structures.

Conclusion: Our study underscores the importance of *K. pneumoniae* in the ISS, and its potential positive and negative interactions with other microbes, including potential pathogens. This integrated modeling approach, combined with experiments, demonstrates the potential for understanding the organization of other such microbiomes, unravelling key organisms and their interdependencies.

Keywords: Microbial communities, Space microbiome, Community modeling, Network biology, Metabolic networks

Background

Microorganisms are ubiquitous and exist in diverse communities around us. They form complex dynamic assemblages in every ecosystem, and their interactions shape the biotic and abiotic environments [1–3]. Beyond natural environments such as the soil or the ocean, microorganisms abound in all human habitats, where they directly impact human health [4]. The human-made

*Correspondence: kraman@iitm.ac.in; kjvenkat@jpl.nasa.gov

[3] NASA Jet Propulsion Laboratory, California Institute of Technology, Pasadena, M/S 89-2, 4800 Oak Grove Dr, Pasadena, CA CA 91109, USA
[4] Department of Biotechnology, Bhupat and Jyoti Mehta School of Biosciences, Indian Institute of Technology Madras, Chennai 600 036, India
Full list of author information is available at the end of the article

International Space Station (ISS) is a unique and controlled system to study the interplay between the human microbiome and the microbiome of their habitats. The ISS is a hermetically sealed closed system, yet it harbors many microorganisms that survive extreme environmental conditions such as microgravity, radiation and elevated CO_2 levels [5–8]. Recent studies have demonstrated the unique link between crew member microbiomes and surface microbiomes on the ISS [9]. These microorganisms might have been brought into the ISS via routine payloads and astronauts [9].

Several studies have focused on microbial isolation [10] and molecular microbial community analyses of the ISS microbiome, through experiments performed on vacuum filter debris [11], high-efficiency particle arrestance (HEPA) filters [12, 13], the ISS environmental surfaces [8, 14] and astronauts' microbiome [9]. A recent report using a shotgun metagenomic sequencing approach on intact cells of the ISS environmental microbiome revealed the succession and persistence of certain microbial populations on the ISS environmental surfaces [15]. The study posited a dominant, viable presence of Biosafety Level – 2 (BSL-2) pathogens such as *Klebsiella pneumoniae, Staphylococcus aureus, Enterococcus faecalis* and *Salmonella enterica* (Figure S1).

K. pneumoniae is well-known for its ability to cause pneumonia and other nosocomial infections and is largely studied for its known resistance to a wide spectrum of antibiotics, such as carbapenems, and its hypervirulence [16–20]. The present study is motivated by the evidence presented about the dominance of *K. pneumoniae* at multiple locations of the ISS, its succession over time [15], and the potential clinical implications it could have on the health of the astronauts inhabiting the ISS.

Metabolic interactions are a key driver in shaping microbial communities [21]. Studying these metabolic interactions can be instrumental in understanding the interplay between various microorganisms in diverse communities [22–24]. Genome-scale metabolic modeling is a powerful tool to study and understand microbial metabolism [25]. These modeling approaches capture in detail, the known metabolic reactions happening in a microorganism, along with the enzymes that catalyze them, representing them in a mathematical form amenable to simulations [26]. Beyond single microorganisms, metabolic modeling can also be extended to study microbial communities; many paradigms have been developed, including those based on graph theory, and constraint-based modeling, as reviewed elsewhere [27, 28].

In this study, we leverage the metagenome datasets that have captured the microbial composition of the ISS surfaces [15] to specifically predict how various species in

these communities can influence one another's metabolism, leading to mutually beneficial interactions and stable microbiomes. In particular, we focus our study on *K. pneumoniae* and its coexisting species, to elucidate the possible underlying metabolic interactions that drive the structure of these communities. Through a combination of a systems-based graph-theoretical approach, MetQuest [29, 30], and a constraint-based community modeling approach, SteadyCom [31], we illustrate the central role of metabolic interactions and dependencies in shaping the ISS microbiome.
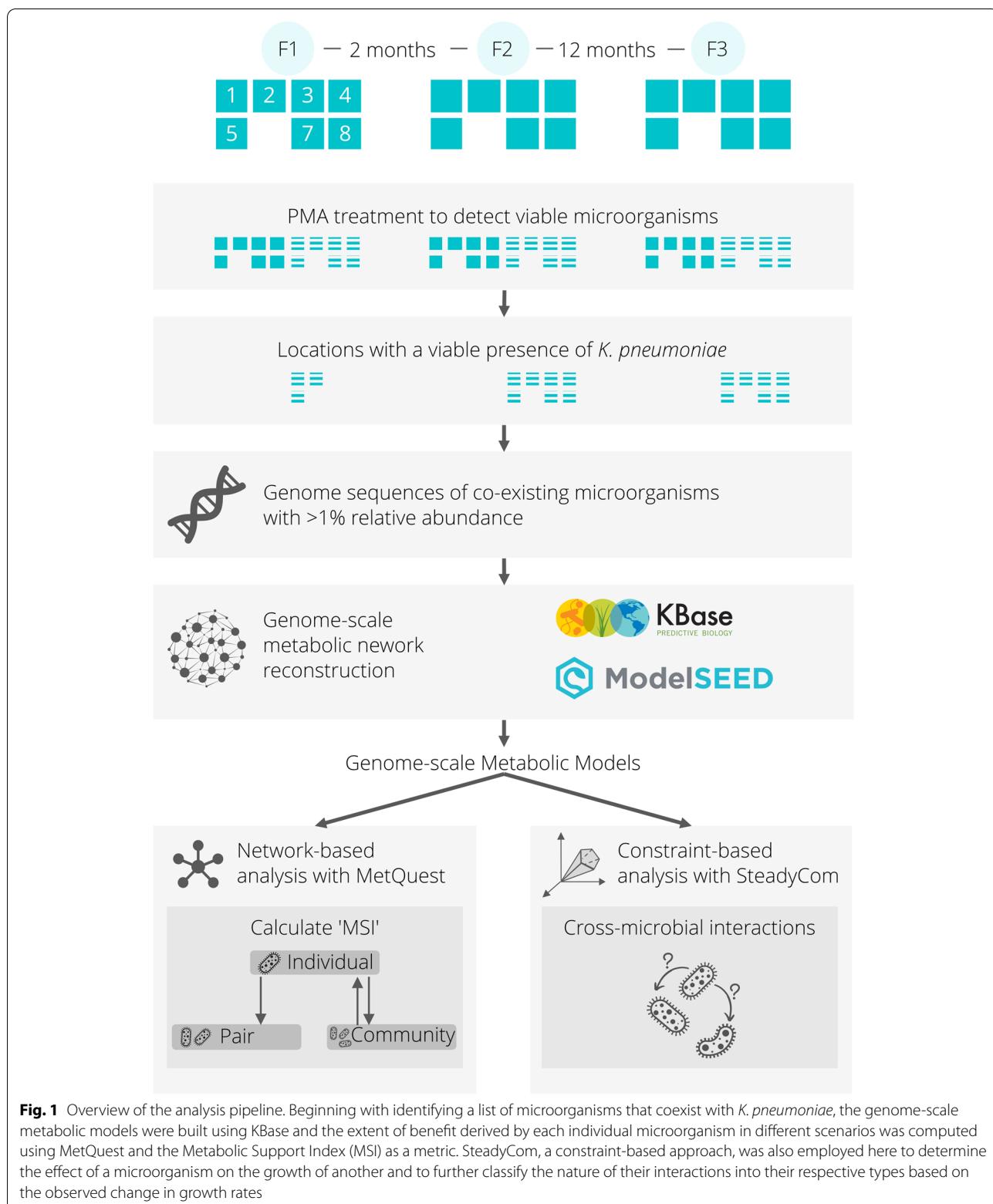
Methodology

In this study, a two-pronged computational approach was adopted to investigate and decipher the prevailing microbial interactions in the ISS. In the first graph-based approach [29], bipartite graphs were created to represent the metabolic networks of microorganisms taken individually, as well as when in pairs or larger communities. The metabolic networks underlying the organisms were represented as bipartite graphs, where two groups of nodes represent metabolites and reactions, and directed edges connect substrates to reactions and reactions to products. These networks were used to identify possible metabolic dependencies between different microorganisms. In the second constraint-based approach [31], microbial growth rates were predicted, individually and in communities, to gauge the nature of their interactions, as we describe in the following sections. Figure 1 shows a broad overview of the approach of this study, outlining the steps beginning with the identification of microorganisms coexisting with *K. pneumoniae* to various metabolic network analyses.

Data

Microbial abundances associated with samples taken across three flights at eight ISS locations were previously measured using metagenomic sequencing [15]. Among eight locations, only seven locations yielded measurable metagenomics data. In the present study, the data were further pruned such that only shotgun metagenome sequences associated with propidium monoazide (PMA)-treated samples that recorded a presence of *K. pneumoniae* were retained. The PMA-treatment removed naked DNA and dead cells, thus retaining sequences associated with viable and intact cells only [32]. Further, only microorganisms that were found to coexist with *K. pneumoniae* with >1% relative abundance at the location were used in this study.

For this study, the available whole-genome sequences (WGS) of microorganisms from the ISS, which were compatible with KBase [33] along with reference genomes for the relevant microorganisms taken from the

Fig. 1 Overview of the analysis pipeline. Beginning with identifying a list of microorganisms that coexist with *K. pneumoniae*, the genome-scale metabolic models were built using KBase and the extent of benefit derived by each individual microorganism in different scenarios was computed using MetQuest and the Metabolic Support Index (MSI) as a metric. SteadyCom, a constraint-based approach, was also employed here to determine the effect of a microorganism on the growth of another and to further classify the nature of their interactions into their respective types based on the observed change in growth rates

NCBI database, were collected. The RefSeq and GenBank accession identification numbers, along with the underlying reasoning for the choice of these sequences, are provided in Supplementary Table S1. Although the relative abundance of *Pantoea* sp. PSNIH2 was >1% in some of the locations considered in this study, as its reference genome sequence was removed from the NCBI database, at the time of this study, this microorganism therefore had to be excluded. Metabolic models were constructed for the 52 microorganisms using ModelSEED [34]. The detailed process is elaborated in Supplementary Methods M1. The details of the reconstructions, templates and information about reaction counts are specified in Supplementary Table S2.

Predicting metabolic dependencies in the community
To investigate the microbial interactions underlying the chosen microbial communities of the ISS, MetQuest [29], a graph-theoretic algorithm was first employed. Through a novel dynamic-programming-based enumeration, MetQuest assembles reactions into pathways of a specified size producing a given target from a specified set of source molecules ('seed'). Through a guided breadth-first search, MetQuest can identify all the metabolites that can be traversed from a set of seed metabolites. This functionality was exploited in this study as previously published [30]. Using this algorithm, the present study presents a top-down view of metabolic dependencies in these communities, beginning with predicting the most supportive families, then the most dependent genera, and finally the beneficial and dependent microorganisms by looking at pairs of potentially interacting microorganisms. In each scenario, the extent of benefit derived was calculated using a measure known as the Metabolic Support Index (MSI) [30]. This was also extended to measure the possible support an organism derives from (or provides to) a community where it is present, denoted Community Support Index (CSI).

The composition of the seed metabolites was chosen so as to incorporate the co-factors and coenzymes that would be present in the environment and required by a living cell, and capture the minimal nutrient content offered by the ISS. The minimal medium of each metabolic model was identified by minimizing the components required to achieve a minimum growth rate of 0.1 h^{-1}, using built-in functions in COBRApy [35], namely minimal_medium from the cobra.medium module. This approach was adopted on the premise that each microorganism is capable of individual growth. For each location at each flight, the minimal medium sets corresponding to each constituent microorganism were pooled together to form a consolidated medium. Additionally, a base set of co-factors and coenzymes were added to each of these sets. The same medium was used for both the graph-based and constraint-based analyses. Supplementary Table S3 contains the list of all such metabolites.

Pairwise interactions
For a pair of microorganisms, *A* and *B*, MSI is calculated as follows:

$$\text{MSI}(A|A \cup B) = 1 - \frac{n_{stuck,A|A\cup B}}{n_{stuck,A|A}} \tag{1}$$

Here, $n_{stuck,\ A|A\cup B}$ refers to the number of stuck reactions in *A*, when present in the community alongside *B*, while $n_{stuck,\ A|A}$ refers to the number of stuck reactions in *A*, when it is present in isolation. Individual bipartite graphs were constructed ($n=52$), and the stuck reactions were first determined for every individual microorganism in the dataset, using the MetQuest algorithm as described above, which provided insight into the intrinsic metabolic capabilities of each individual microorganism. Following this, for every pair of coexisting microorganisms that may potentially interact, bipartite graphs were constructed for the two-member community ($n=426$), and the stuck reactions were determined for each constituent member of each community, in a flight-location-specific approach ($n=761$), to derive the effect of its partner by virtue of being in this community, through the calculation of the MSI.

Building further on these interactions, as captured by the MSIs between various microbial pairs, microbial association networks were constructed and visualized using Cytoscape [36]. These networks capture the extent to which a microorganism is able to relieve the stuck reactions of another through metabolic exchanges.

Higher-order interactions
The enhancement of metabolic capabilities rendered by a microorganism(s) by virtue of it thriving in a community was derived from the MSI, here referred to as the community support index (CSI). The CSI, denoted $CSI_{A\to\tilde{A}}$ throughout this manuscript, was calculated as the fraction of reactions relieved in the rest of the community over the reactions 'stuck' in the same in the presence of the microorganism. For a community *X* and an inhabitant microorganism, or family of microorganisms, *A*, the effect of *A* on the rest of the community $\tilde{A} = (X-A)$, where $\tilde{A}$ denotes the rest of the community *X* devoid of microorganism/family *A*, is computed as follows:

$$\text{CSI}\left(\tilde{A}|X\right) = 1 - \frac{n_{stuck,\tilde{A}|X}}{n_{stuck,\tilde{A}|\tilde{A}}} \tag{2}$$

Here, $n_{stuck,\tilde{A}|\tilde{A}}$ refers to the number of stuck reactions in the community X without microorganism A for the given set of seed metabolites. A reaction is considered stuck when it does not have the necessary precursors for the reaction to happen. In other words, these are reactions that cannot occur under the present conditions, without extraneous help in terms of other metabolites from other microorganism(s), or the environment itself. Similarly, $n_{stuck,\tilde{A}|X}$ refers to the number of reactions in $\tilde{A}$ that remain stuck, even in the presence of A. We consider only internal reactions (as against transport or extracellular reactions) while computing these numbers.

For each of the sites considered in this study, bipartite graphs were first constructed ($n = 129$) for communities devoid of one constituent microorganism, and their respective stuck reactions were determined in the appropriate environment (i.e., the seed metabolites described above and listed in Supplementary Table S3). This approach provided insight into the intrinsic metabolic capabilities of each community devoid of that microorganism. Following this, a total 11 bipartite graphs were constructed, taking into consideration all inhabitant microorganisms of a particular site. The stuck reactions were determined for each community to gather the effect of the interactions by calculating the $CSI_{A \to \tilde{A}}$. A $CSI_{A \to \tilde{A}}$ of unity indicates that A completely supports $\tilde{A}$ and relieves all its stuck reactions, whereas a value of zero indicates that A has no effect on $\tilde{A}$.

Microorganisms could potentially be metabolically similar, and therefore redundant to the community, offering little or no metabolic support individually. Therefore, microbial interactions were also studied by grouping them by their respective families ($n = 7$), at each location. The metabolic support provided by groups of microorganisms (e.g., a family) can be readily computed by replacing A in $X - A$ with the set of microorganisms comprising the family in Eq. (1).

It is also possible to estimate the community benefit, in terms of enhancement of metabolic capabilities, an individual microorganism might receive by virtue of it thriving in a community. Here, the CSI, denoted $CSI_{\tilde{A} \to A}$, was calculated as the fraction of reactions relieved in the microorganism when in a community assemblage over the reactions stuck in the individual. For a community X and an inhabitant microorganism A, the effect of the rest of the community $\tilde{A}$ on A is computed as follows:

$$\text{CSI}(A|X) = 1 - \frac{n_{stuck,A|X}}{n_{stuck,A|A}} \tag{3}$$

The $CSI_{\tilde{A} \to A}$ thus captures the 'benefit' a microorganism or a group of microorganisms receives from another microorganism or group, by virtue of its stuck reactions being relieved via metabolic exchanges with its coexisting microorganisms. For clarity, all CSIs and MSIs have been represented as percentages.

Determining the nature of interactions

Microbial interactions have major relevance in building and shaping the community. Based on the effects a microorganism has on another, the interactions can be categorized into six types, namely amensalism, commensalism, competition, neutralism, mutualism and parasitism [37]. The present study reports a constraint-based community modeling study using the algorithm, SteadyCom [31].

SteadyCom [31] was employed to determine the biomass production rates of all microorganisms that are a part of a community under steady state. The seed metabolites described earlier, in the network-based approach were used here as the medium (see Supplementary Table S3). The lower bounds of the exchange reactions for the uptake of these metabolites were constrained to -10 mmol/gDW-h [38]. Joint models were then created for all pairs of microorganisms that can potentially interact by virtue of being at the location at that point in time. These joint models were optimized using SteadyCom [31] to find the individual biomass rates when existing as a community.

The growth rate observed for each microorganism in community was compared with that observed for the individual microorganism. A 10% or higher increase or decrease in growth rate, when in a community, was taken to be a significant effect [39]. The interactions were accordingly classified into the types listed above. The equation defined below was used to determine the effect of microorganism B on A, in a two-membered community constituting A and B.

$$\text{Effect of } B \text{ on } A = \frac{v_{bio,AB} - v_{bio,A}}{v_{bio,A}} \tag{4}$$
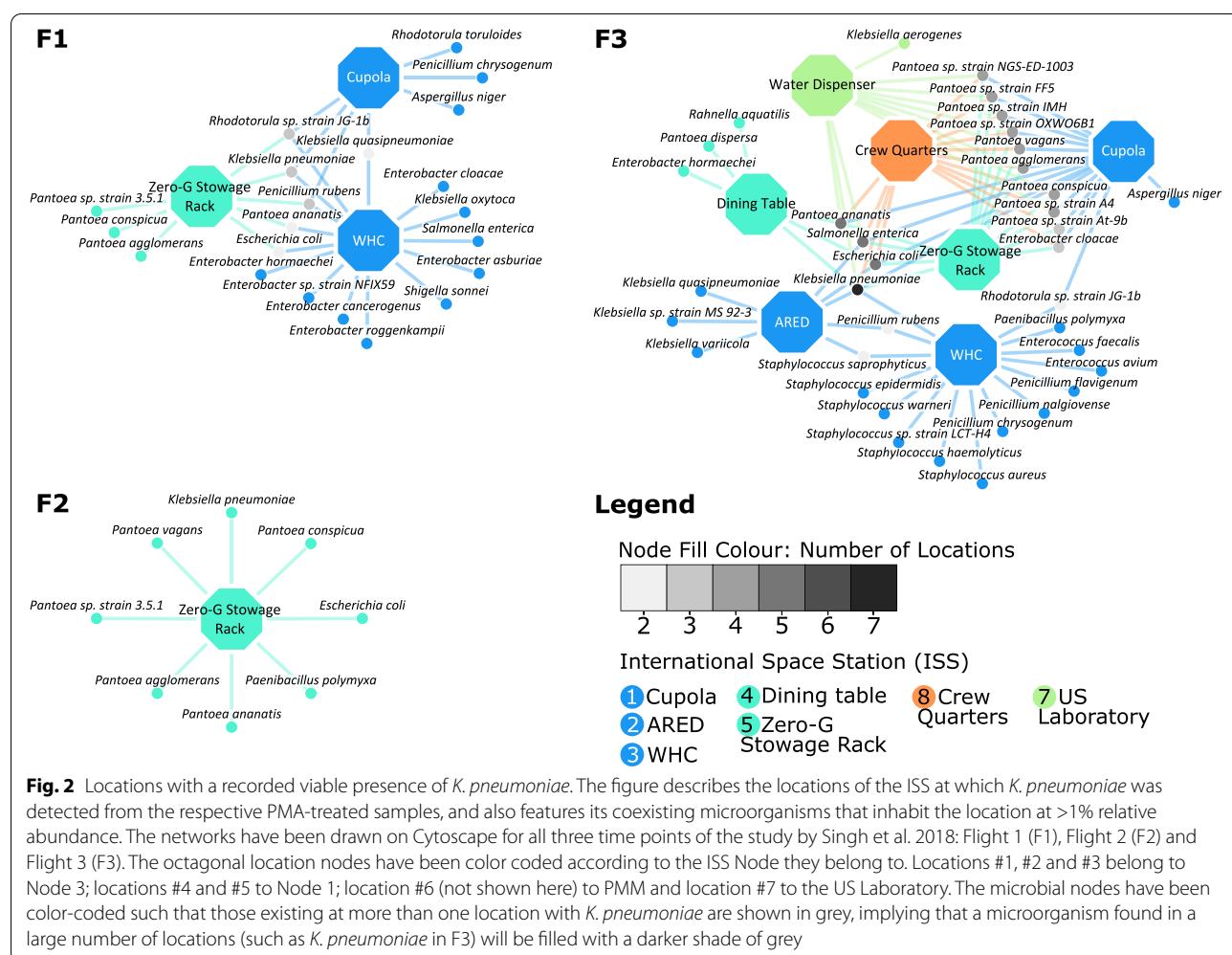
where $v_{bio,\,AB}$ is the community biomass production rate of AB and $v_{bio,\,A}$ is the biomass production rate of A.

Depending on the value (positive [+], negative [−], or neutral [0]) obtained, the interaction was classified as mutualism (the effect of B on A, and the effect of A on B, both being positive, i.e., +, +), neutralism (effects on each other being not significant, denoted 0,0), competition (a negative effect on each other, denoted by −,−), amensalism (−,0 and 0,−), commensalism (0,+ and +,0), and parasitism (−,+ and +,−).

K. pneumoniae and *A. fumigatus* interactions

Overnight grown cultures of *K. pneumoniae* (10^6 cells per 100 μL) and purified conidia of *A. fumigatus* (10^6 per 100 μL) were either mixed or grown alone in a 10-mL sterile potato extract (0.4%; w/v) dextrose (2%; w/v) liquid medium and

Fig. 2 Locations with a recorded viable presence of *K. pneumoniae*. The figure describes the locations of the ISS at which *K. pneumoniae* was detected from the respective PMA-treated samples, and also features its coexisting microorganisms that inhabit the location at >1% relative abundance. The networks have been drawn on Cytoscape for all three time points of the study by Singh et al. 2018: Flight 1 (F1), Flight 2 (F2) and Flight 3 (F3). The octagonal location nodes have been color coded according to the ISS Node they belong to. Locations #1, #2 and #3 belong to Node 3; locations #4 and #5 to Node 1; location #6 (not shown here) to PMM and location #7 to the US Laboratory. The microbial nodes have been color-coded such that those existing at more than one location with *K. pneumoniae* are shown in grey, implying that a microorganism found in a large number of locations (such as *K. pneumoniae* in F3) will be filled with a darker shade of grey

grown under normal and simulated microgravity conditions using high aspect ratio vessel (HARV; Synthecon inc., Houston, TX) culturing units [40]. The autoclavable HARVs provided oxygenation to the culture media via their large-diameter gas permeable membrane. The HARVs with microbes were incubated at 30 °C; 150 rpm, for 48 h. HARVs were run in parallel in both horizontal rotation (normal gravity control) and vertical rotation (simulated microgravity) orientation during growth. After growth, the bacterial and fungal cells were harvested, then fixed by incubating the cells in 2.5% glutaraldehyde in 0.1M Sodium Cacodylate (Sigma) buffer at 4 °C for 1 h for scanning electron microscopy (SEM) study. Samples were then washed in 0.1M sodium cacodylate buffer three times. Fixed cells were then dehydrated in isopropyl alcohol (IPA, Sigma), using a stepped series of increasing concentrations (50%, 70%, 80%, 90%, 95 to 100%). Each step consisted of a 10-min incubation at 4 °C, followed by 3 x replacements with 100% IPA, and finally stored at 4 °C. Samples were critically point dried in an Automegasamdri 915B critical point dryer (Tousimis, Rockville, MD). Samples were attached in SEM stubs with carbon tape (Ted Pella Inc., Redding, CA), followed by carbon coating with a Leica EM ACE600 Carbon Evaporator (Leica, Wetzlar, Germany) to a thickness of ~12nm. SEM analysis was performed with an FEI Quanta 200F (Thermo Fisher, Waltham, MA).

Results

Data acquisition and genome-scale metabolic network reconstruction

According to the data published by Singh et al. 2018 [15], among the PMA-treated samples, reads of *K. pneumoniae* were detected in a total of 11 sites—locations #1, #2, and #5 in Flight 1; location #5 in Flight 2; and locations #1, #2, #3, #4, #5, #7, and #8 in Flight 3 (Fig. 2). The relative abundances of microorganisms were calculated at the respective sites, and upon further pruning of this data to include solely those with >1% abundance, a total of 50 different strains of microorganisms that coexist with

K. pneumoniae at varied locations and time points were chosen for further study.

Analysis of the diversity of these microorganisms at each of these locations over time (Fig. 2) reveals the following trends. In Flight 1, among the three locations that were colonized by *K. pneumoniae*, there was an observed dominance of fungi in location #1, *Enterobacteriaceae* in location #3, and *Erwiniaceae* in location #5. In Flight 2, *K. pneumoniae* was documented to be present only in location #5, coexisting with extant and dominant *Erwiniaceae*, a member from the *Enterobacteriaceae* family and another from the *Paenibacilleae* family. In Flight 3 however, *K. pneumoniae* spread across the ISS, inhabiting nearly all sampled locations. Additionally, many more members of *Erwiniaceae*, specifically the *Pantoea* genus, emerged into view at a majority of these locations, as shown in Fig. 2. Further, with the exception of *A. niger* and *Rhodoturula* sp. strain JG-1b, all fungi considered in the dataset appear to be concentrated in location #3. Location #3 is also dominated by a large number of *Staphylococcaceae*. The list of microorganisms, along with their relative abundances at each location in each flight, is provided in Supplementary Table S4.

Enterobacteriaceae are pivotal contributors to community metabolism

Through a 'leave-one-out' approach, microorganisms were knocked out one at a time from the community to estimate the extent of benefit provided by that single microorganism to the remaining coexisting microorganisms. From the analysis, it was evident that some microorganisms do have an influence on the metabolic capabilities on the rest of the community, albeit low in most cases. Notable among these, were *P. rubens* at location #3 during Flight 3 ($CSI_{A \to \tilde{A}}$ = 1.15%), and at locations #2 ($CSI_{A \to \tilde{A}}$ = 0.40%) and #5 ($CSI_{A \to \tilde{A}}$ = 0.36%) during Flight 1, and *K. oxytoca* at location #2 in Flight 1 ($CSI_{A \to \tilde{A}}$ = 0.49%) (Supplementary Table S5 and Supplementary Figure S2).

These low values of $CSI_{A \to \tilde{A}}$ are expected, given the possible high metabolic overlap between members within a community, thereby rendering individual organisms less important to a community. To examine this, we grouped organisms based on their phylogenetic affiliation, and removed these groups, one at a time, from the community, to study the importance of a given family to the community.

Overall, with respect to the locations considered in this study, the *Enterobacteriaceae* family comprising species of the *Klebsiella*, *Escherichia*, *Salmonella*, *Shigella*, and *Enterobacter* genera, was often found to be the most beneficial of all clusters, with the highest $CSI_{A \to \tilde{A}}$s in six out of a total eleven communities under study (Fig. 3 and Supplementary Table S6), five of which were in Flight 3. With regards to the remaining five communities, *Trichocomaceae* have the highest $CSI_{A \to \tilde{A}}$s at locations #2 and #5 during Flight 1, *Erwiniaceae* have the highest $CSI_{A \to \tilde{A}}$s at location #1 in Flight 3 and at location #5 during Flight 2, and *Paenibacillaceae* has the highest $CSI_{A \to \tilde{A}}$ at location #2 in Flight 3. Here, *A* refers to the family of microorganisms that provides metabolic support.

Pantoea species thrive in the support of the microbiome

The $CSI_{\tilde{A} \to A}$ of an individual microorganism in the presence of its coexisting microorganisms was calculated to gain insight into the combined effect of the community on an individual. The $CSI_{\tilde{A} \to A}$ values of *Pantoea* were found to be among the highest (Supplementary Table S7 and Fig. 4), indicating that these species are benefitted to a comparatively greater extent from the remaining members of the community. Across all locations and flights in the dataset, the $CSI_{\tilde{A} \to A}$ values of these species ranged between 0 and 6.52%, wherein the values at the lower end were predominantly observed in those *Pantoea* species found at location #1 in Flight 3. *P. vagans* was found to exhibit the highest dependency amongst all the *Pantoea*, at location #5 in Flight 2 (Fig. 4).
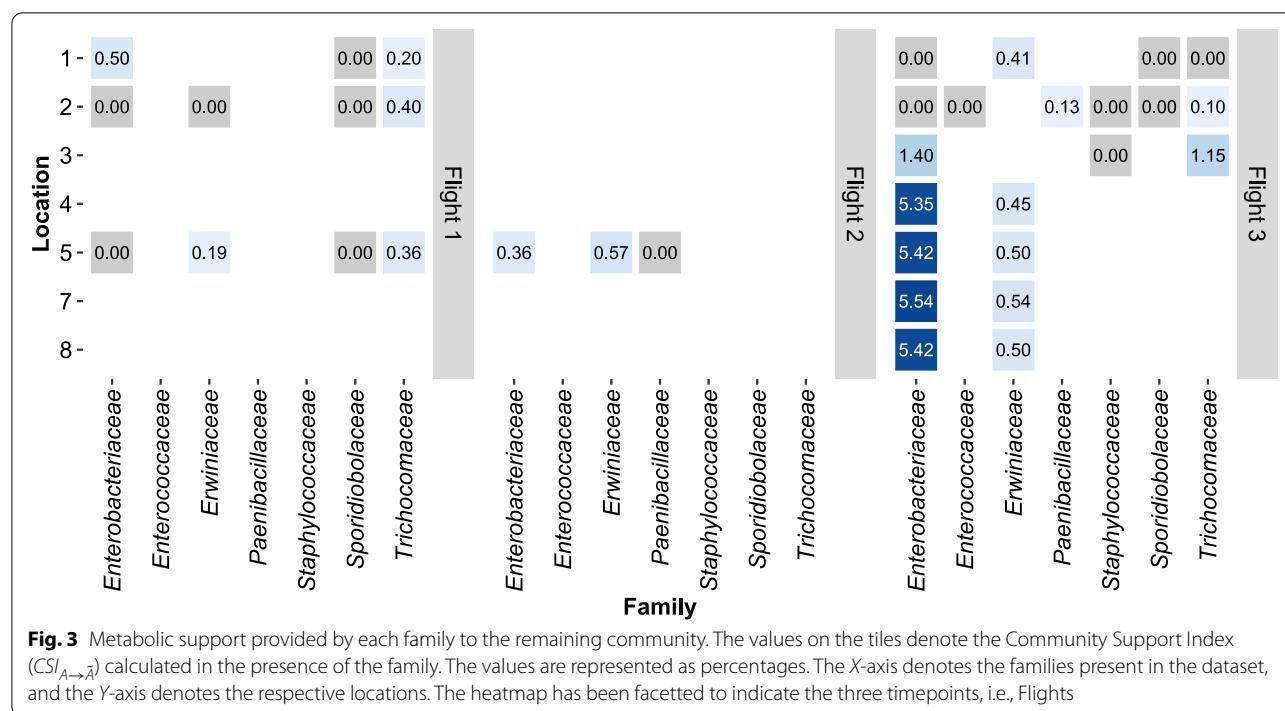
With the exception of *E. coli* and *S. enterica*, the $CSI_{\tilde{A} \to A}$ values of other *Enterobacteriaceae* fell in the range of 0–0.91%, suggesting an overall lower dependence of members of the *Enterobacteriaceae* on their coexisting microorganisms (Fig. 4). *K. pneumoniae* showed no dependency ($CSI_{\tilde{A} \to A}$ = 0%) in six out of the 11 locations that they were found. In addition, *S. enterica* exhibited the highest community dependence amongst all microorganisms in consideration, with a $CSI_{\tilde{A} \to A}$ = 8.79% at location #3 during Flight 3, and along with *E. coli*, showed high $CSI_{\tilde{A} \to A}$ values (Fig. 4).

Analysis across the three flights at location #5 reveals that four out of five organisms present at all instances are benefitted to a lesser extent in Flight 1 compared to Flights 2 and 3 (Fig. 4 and Supplementary Table S7).

K. pneumoniae are beneficial *to* its coexisting microorganisms

In every community, microorganisms exchange metabolites, influencing one another's growth and survival. We performed a pairwise analysis of a total of 761 flight-location-specific communities to identify how every pair of microorganisms interacts with one another, at a given location, during a given flight, and through various metabolic exchanges support each other.

In communities with *K. pneumoniae* and a member outside of the *Enterobacteriaceae*, the MSI values in the

Fig. 3 Metabolic support provided by each family to the remaining community. The values on the tiles denote the Community Support Index ($CSI_{A \to \bar{A}}$) calculated in the presence of the family. The values are represented as percentages. The *X*-axis denotes the families present in the dataset, and the *Y*-axis denotes the respective locations. The heatmap has been facetted to indicate the three timepoints, i.e., Flights

presence of *K. pneumoniae* were found to fall in the range of 0–6.46%. Most *Pantoea* species were found to be highly dependent on *K. pneumoniae*, with MSIs at the higher end (4.41–6.46%) of the spectrum (Supplementary Table S8). With the exception of *E. coli* and *S. enterica*, the MSI values of all other *Enterobacteriaceae* members were found to be 0% in the presence of *K. pneumoniae* (Supplementary Figures S3 and S4). Out of 118 pairs, *K. pneumoniae* was found to have a non-zero MSI value in only nine such pairs. In these nine pairs, the other interacting member belonged to a species of the *Penicillium* genus.

Since *K. pneumoniae* was present across the three flights only at location #5, the corresponding microbial association networks were constructed to gain insights into microbial interaction patterns over time (Fig. 5). In Flight 1, fungi such as *P. rubens* and *Rhodotorula* sp. JG-1b are prevalent and shown to decline in abundance over time (Flight 2 and Flight 3). On the contrary, members of the *Panteoa* genus were observed to dominate this location over time, with many more *Pantoea* species surfacing. In agreement with earlier results discussed, many species of the *Enterobacteriaceae* family shown here such as *K. pneumoniae* and *E. cloacae*, were beneficial to members of the *Erwiniacea* family to a great extent (Fig. 5).

## Constraint-based modeling suggests the domination of amensalistic and parasitic interactions

The graph-theoretic approaches described earlier do not explicitly account for the growth of microorganisms

in the presence of one another or their rates, although a higher MSI does point towards a possible higher biomass in the community [30]. Complementary to the above approaches, constraint-based modeling approaches such as SteadyCom [31] can shed light on the ability of microorganisms to grow in a steady-state. Based on these predicted growth rates, it is also possible to classify the nature of the interaction between various pairs of microorganisms [37].

A total of 761 flight-location-specific pairs of microorganisms were studied. Among these, 458 pairs exhibited amensalism and 166 were predicted to be parasitism. Of the remaining, 48 were commensal, 36 were competitive, 34 were mutualistic and 19 were neutral.

Looking closely into the nature of interactions of *K. pneumoniae* and its coexisting microorganisms, in 118 such pairs, 72 were predicted to be amensal, 14 commensal, 13 involved in competition, 10 were parasitic interactions, seven were mutual and two were neutral. In communities with the *Enterobacter* species, *K. pneumoniae* was involved in amensalistic interactions as observed across all such flight-location pairs. While in the interactions with *E. cancerogenus* and *Enterobacter* sp. strain NFIX59, the growth rate of *K. pneumoniae* was predicted to decrease, in the interactions with all other *Enterobacter* species, there was no significant effect on the predicted growth rate of *K. pneumoniae*.

In eight out of nine flight-location-specific communities of *K. pneumoniae* with *E. coli*, *E. coli* was predicted
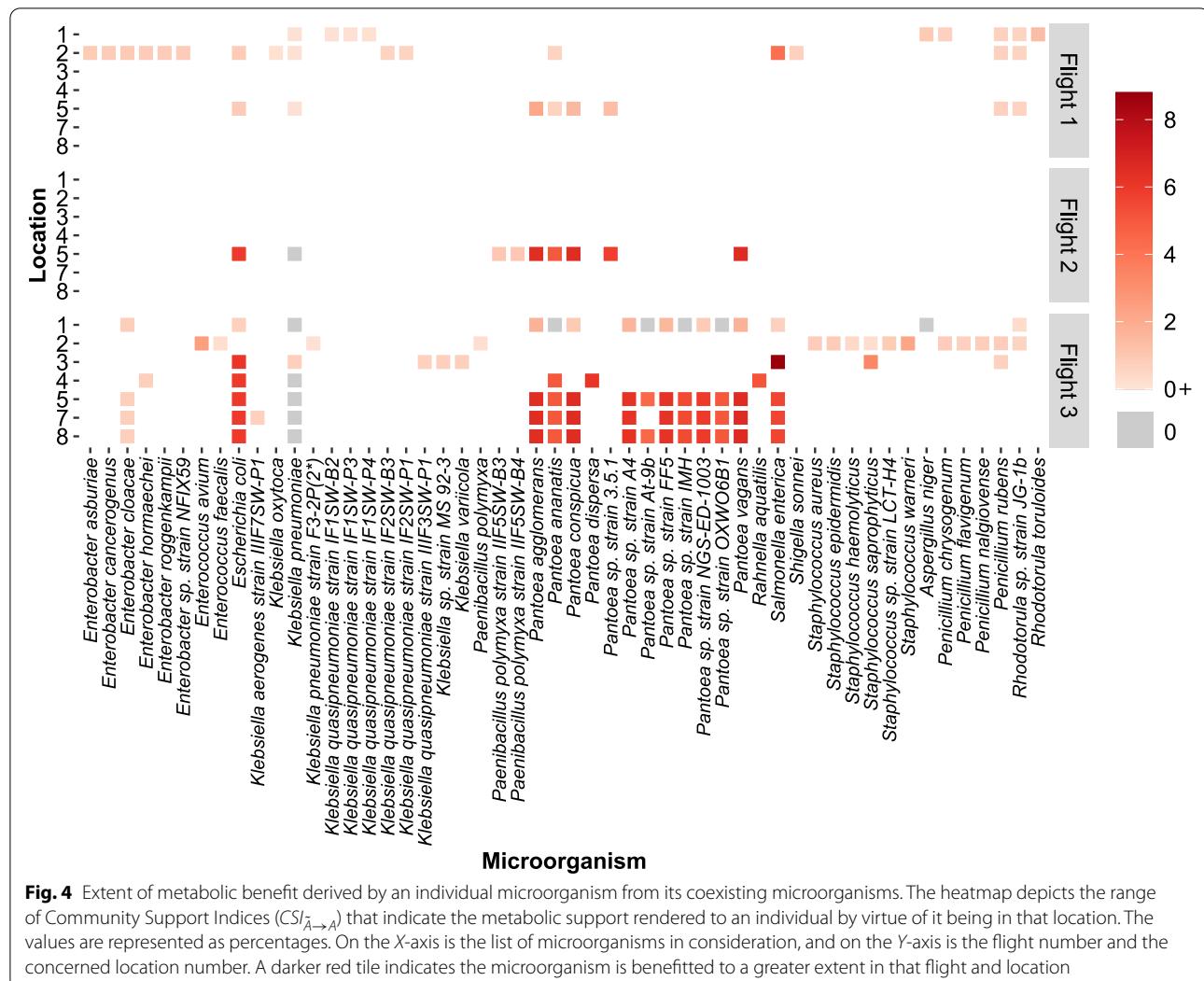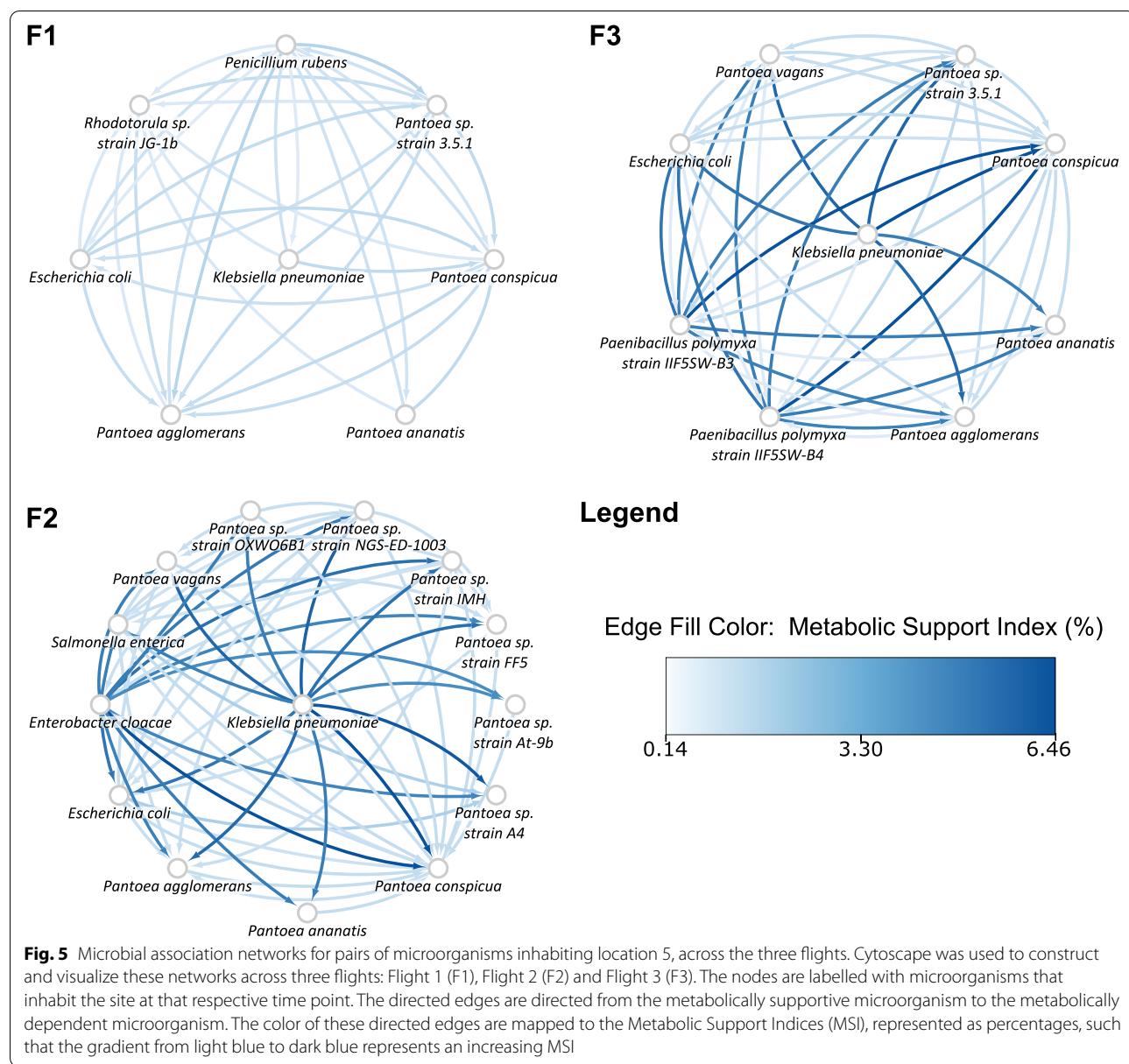
Fig. 4 Extent of metabolic benefit derived by an individual microorganism from its coexisting microorganisms. The heatmap depicts the range of Community Support Indices ($CSI_{\bar{A}\rightarrow A}$) that indicate the metabolic support rendered to an individual by virtue of it being in that location. The values are represented as percentages. On the *X*-axis is the list of microorganisms in consideration, and on the *Y*-axis is the flight number and the concerned location number. A darker red tile indicates the microorganism is benefitted to a greater extent in that flight and location

to have no significant change in growth rate while that of *K. pneumoniae* was predicted to decrease, suggesting an amensalistic interaction. Further, in Flight 3, at location #3, *E. coli* was predicted to be parasitic towards *K. pneumoniae*. In the interactions with *S. enterica*, in four out of the six locations, the growth rate of *K. pneumoniae* was decreased in its presence, whereas that of *S. enterica* was increased, resulting in a parasitic interaction. This is in accordance with the previously observed high MSI values at locations #3, #5, #7, and #8 during Flight 3. In the other cases during Flight 1 at location #2 and Flight 3 at location #1, the interaction was predicted to be amensalistic, wherein the growth rate of *K. pneumoniae* was reduced.

With other *Klebsiella* species, the interactions were predicted to be predominantly amensalistic, with the growth rate of *K. pneumoniae* reduced, except in the interaction with *Klebsiella* sp. strain MS 92-3, where the reverse was observed. *K. pneumoniae* was predicted to be parasitic towards *K. aerogenes* strain IIIF7SW-P1.

The interactions with *Pantoea* species, such as *P. agglomerans*, *P. conspicua*, *Pantoea* sp. strain 3.5.1, *Pantoea* sp. strain A4, *Pantoea* sp. strain At-9b, *Pantoea* sp. strain FF5, *Pantoea* sp. strain NGS-ED-1003, *Pantoea* sp. strain OXWO6B1 and *P. vagans*, were amensalistic with a decreased growth rate of the *Pantoea* species, in all cases except in Flight 3 at location #1, where the interactions were predicted to be competitive. Interactions with *P. ananatis* however were found to be commensal, with an observed increased growth rate. *P. dispersa* and *Pantoea* sp. strain IMH were found to compete with *K. pneumoniae* at their coexisting locations (Fig. 6 and Supplementary Table S9).
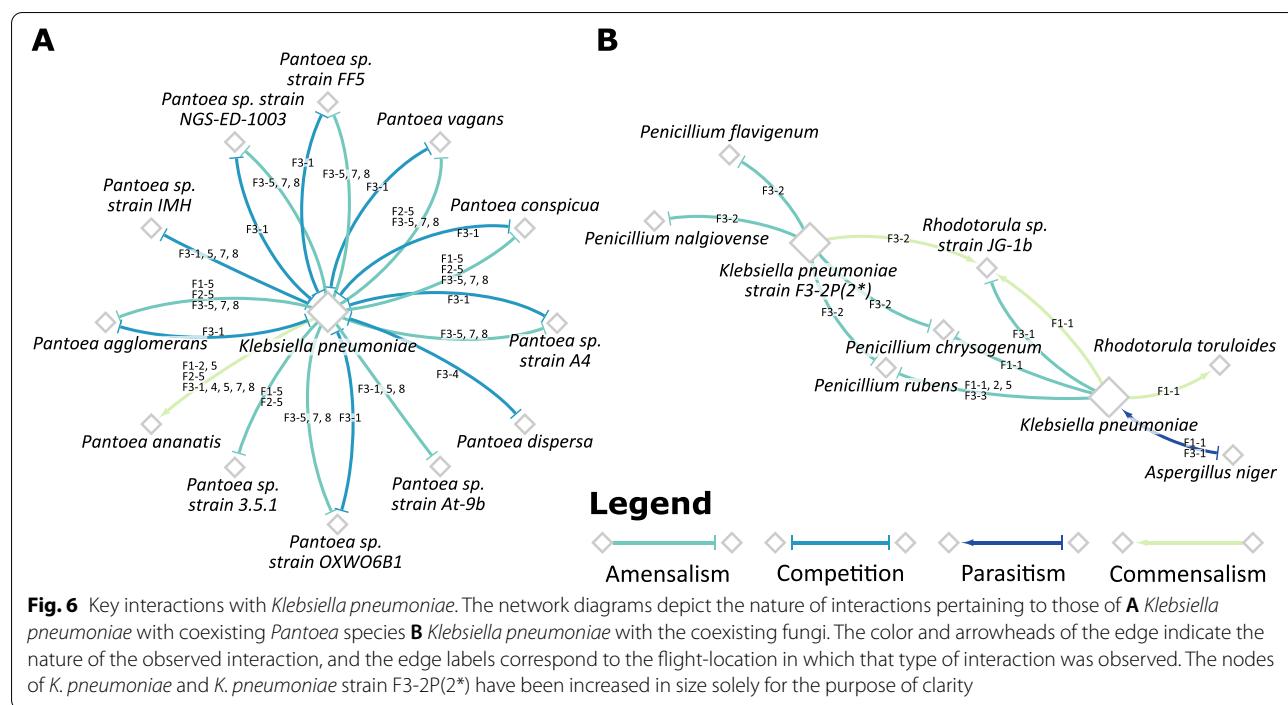
Staphylococcus sp. in Flight 3 at location #2 were found to be mutualistic with *K. pneumoniae* strain F3-2P(2*), with the exception of *S. saprophyticus* that was observed to be involved in commensalism. During Flight 3, location #3 however, this interaction of *S. saprophyticus* with *K. pneumoniae* was predicted as mutualistic

Fig. 5 Microbial association networks for pairs of microorganisms inhabiting location 5, across the three flights. Cytoscape was used to construct and visualize these networks across three flights: Flight 1 (F1), Flight 2 (F2) and Flight 3 (F3). The nodes are labelled with microorganisms that inhabit the site at that respective time point. The directed edges are directed from the metabolically supportive microorganism to the metabolically dependent microorganism. The color of these directed edges are mapped to the Metabolic Support Indices (MSI), represented as percentages, such that the gradient from light blue to dark blue represents an increasing MSI

(Supplementary Table S9). This observed change in the nature of interactions may perhaps be attributed to the differences in the simulated medium compositions at the different locations.

The interactions of *K. pneumoniae* with *A. niger* were observed to be parasitic, with an observed decreased growth rate of *A. niger* and an increased growth rate of *K. pneumoniae*. With *Penicillium* species, *K. pneumoniae* had an amensalistic effect on them, resulting in their decreased growth rates. The interactions with *Rhodotorula* sp. strain JG-1b were found to depend on the flight and location in which they coexisted. During Flight 1, at location #1, an increased growth rate

was observed in *Rhodotorula* sp. strain JG-1b, whereas there was no significant effect on that of *K. pneumoniae*, thereby suggesting a commensal interaction. In locations #2 and #5, however, a neutral interaction was predicted, with no significant change in growth rates of either species. In Flight 3, *K. pneumoniae* was observed to be amensalistic towards *Rhodotorula* sp. strain JG-1b at location #1 and commensal at location #2. *K. pneumoniae* increased the growth rate of *R. toruloides* in Flight 1 at location #1 (Fig. 6 and Supplementary Table S9). Details regarding the nature of interactions of other microorganisms in the community have been delineated in Supplementary Table S9.

Fig. 6 Key interactions with *Klebsiella pneumoniae*. The network diagrams depict the nature of interactions pertaining to those of **A** *Klebsiella pneumoniae* with coexisting *Pantoea* species **B** *Klebsiella pneumoniae* with the coexisting fungi. The color and arrowheads of the edge indicate the nature of the observed interaction, and the edge labels correspond to the flight-location in which that type of interaction was observed. The nodes of *K. pneumoniae* and *K. pneumoniae* strain F3-2P(2*) have been increased in size solely for the purpose of clarity

Detrimental effect of *K. pneumoniae* on *Aspergillus fumigatus*

The parasitic interactions of *K. pneumoniae* on *A. niger* were observed using various microscopic techniques (data not shown). Since *A. niger* is not a pathogenic bacterium, we extensively characterized an ISS isolated *A. fumigatus*, a BSL-2 bacterium, to understand the detrimental effect of *K. pneumoniae*. The scanning electron micrographs confirmed the parasitic effect of *K. pneumoniae* over *A. fumigatus* (Fig. 7). Under normal gravity conditions, *A. fumigatus* was found to be healthy where conidiophore holding vesicle with healthy metulae and phialides harboring conidia were noticed (Fig. 7A), whereas simulated microgravity affected the phialides structure (Fig. 7C) and subsequently conidia-forming cells were not clearly visible. When *K. pneumoniae* was co-cultured with the fungus, under normal gravity conditions, the bacterial cells (artificially colored in red) were shown to destroy the conidia-forming cells and also partially degraded metulae and phialides (Fig. 7B).

Furthermore, when *K. pneumoniae* cells were grown with the fungus and incubated in simulated microgravity conditions, bacterial cells destroyed the fungal structure where only vesicle was seen along with the conidia and phialides, additionally the metulae were disformed and the hyphae (Fig. 7D) appeared to be disfigured compared to those seen in Fig. 7A or B. When co-cultured, the hyphae of *A. fumigatus* appeared to be healthy when grown under normal gravity (Fig. 7B) and mostly dead when exposed to the simulated microgravity (Fig. 7D). The number of

conidia were also less and on top of the conidia-forming cells the fungal morphological architecture changed. These changes were more obvious in microcosm where both *K. pneumoniae* and *A. fumigatus* were co-cultured and exposed to the simulated microgravity (Fig. 7D) than in the setup that were not exposed to simulated microgravity (Fig. 7B). Interpretation of image data was based on careful analysis of multiple images ($n = 100$), not only on a single micrograph of each test condition.

Additional SEM images ($n = 4$ to 6) per condition are provided in Supplementary Figure S5A to S5D. The mixed nature of the microorganisms (bacteria/fungi), the high magnification necessary to resolve the smaller-sized bacterium (creating narrow field of view) and large morphology (mycelium, and conidiophore/conidia) of the fungus combined to prevent adequate SEM observations that would be necessary to reasonably quantify the cells. Thus, statistical analysis was not possible using the SEM approach. This visualization approach demonstrates that *K. pneumoniae* in combination with simulated microgravity negatively influenced the growth of the fungi. Both these bacterial and fungal strains were isolated from ISS and potential detrimental effect of *K. pneumoniae* as predicted by the metabolic model during this study was experimentally demonstrated, confirming the degeneration of *A. fumigatus* morphological architecture. In addition to these morphological modifications, *K. pneumoniae* also reduced the biofilm forming capability of the fungus when grown together (Supplementary Figure S6).
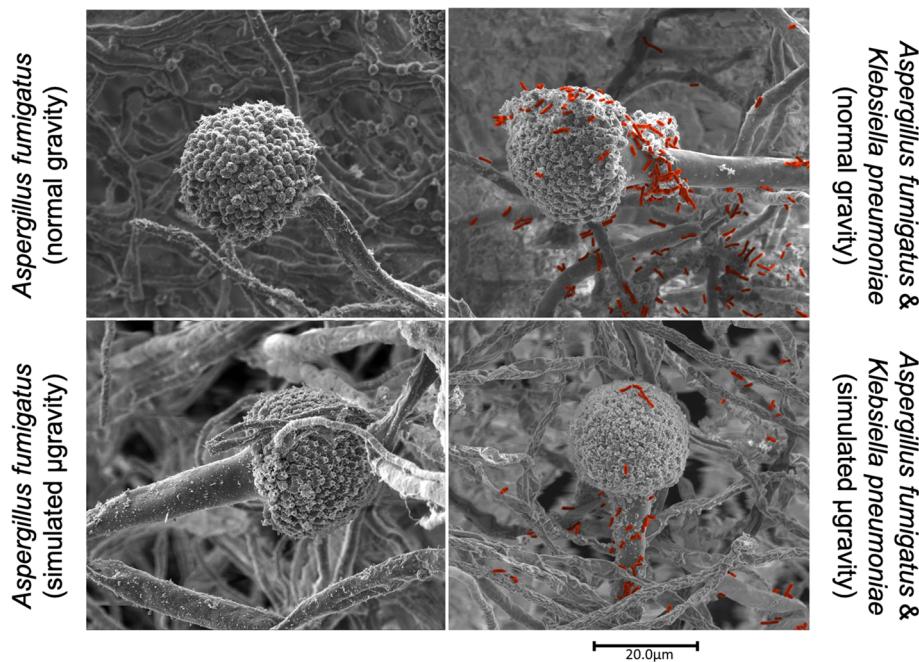
Fig. 7 Antagonistic characteristics of *K. pneumoniae* when co-cultured with *A. fumigatus* under simulated microgravity. **A** *A. fumigatus* grown under normal gravity. **B** Both bacteria and fungus grown under normal gravity. **C** *A. fumigatus* grown under simulated gravity. **D** Both bacteria and fungus grown under simulated gravity. *K. pneumoniae* cells were artificially colored to show their presence on and around fungus culture. These pictures are representative of hundreds of SEM images

Discussion

In this study, we used a metabolic perspective to analyze the ISS microbiome with a focus on *K. pneumoniae*, a BSL-2 human pathogen, and its coexisting microorganisms. In our two-pronged approach, we first used a graph-theoretical approach to unravel the metabolic interdependencies in the microbiome, and we further complemented this with constraint-based analyses, to identify the consequences of microbial interactions on growth. We begin by looking at higher-order interactions in the community and further delve deeper and look at pairwise interactions that have been previously shown to be major drivers of community dynamics [41]. We traverse three taxonomic levels—family, genus and species and provide insights into the keystone species of the community through metabolic network analyses.

The key results of this study are four-fold. First, among the families considered, species belonging to the *Enterobacteriaceae* family were often found to be the most beneficial, among the ISS microbiome. Secondly, *Pantoea* species were predicted to be extensively dependent on their coexisting microorganisms. Third, through metabolic network analysis of microorganisms taken pairwise, *K. pneumoniae* was found to be beneficial to many of its coexisting microorganisms, especially to those species belonging to the *Pantoea*. Fourth, metabolic interactions in

the community broadly fell under the categories of amensalism and parasitism. The parasitic interaction under normal and simulated microgravity between *K. pneumoniae* and *A. fumigatus* was experimentally checked.

Even though <7% of the metagenomic reads of ISS environmental surfaces constituted BSL-2 microorganisms, the dominant and persistent human microbial pathogens were *Pantoea, Klebsiella, Staphylococcus, Erwinia* and *Penicillium* [15]. Among the ISS surfaces, Zero-G Stowage Rack (Location #5) had more *Pantoea* reads compared to other locations of all flights. When metagenomic reads of all BSL-2 microorganisms were compiled, *K. pneumoniae* was found to be persistent and dominant in Zero-G Stowage Rack of all three flights (Fig. 2). In general, *K. pneumoniae* reads were more and dominant in all seven locations sampled in Flight 3. Unlike in Flight 3, *K. pneumoniae* reads were retrieved sparingly in Flight 1 (Cupola and WHC) and Flight 2 (Zero-G Stowage Rack). The cleaning reagent used in ISS consists of benzalkonium chloride, which might be able to eradicate the fungal population; thus fungal succession was not observed, unlike bacterial members which were persistent in the ISS locations examined [42]. It is also documented that *K. pneumoniae* cells were resistant to the quaternary ammonium compound concentration used as cleaning agents in ISS [43].

On applying graph-theoretical algorithms and surveying the microbiome at multiple levels, we predicted that among the families in the dataset, members of the *Enterobacteriaceae* family were perhaps the most beneficial to other microorganisms in the community, whereas in most cases, members of the families such as *Erwiniaceae, Staphylococcaceae* and *Sporidiobolaceae* (yeast) offered little or no additional metabolic benefit to the community. It has been documented that some *Rhodotorula* species produced silver nanoparticles containing antimicrobial properties against a wide variety of Gram-positive and negative microorganisms [44]. The members of the family *Sporidiobolaceae* (*Rhodotorula,* pink yeast) were isolated from the ISS locations [8], their antagonistic and parasitic behavior predicted during this study should be tested against opportunistic microbial pathogens to aid in the development of appropriate countermeasures. Similarly, the amensalism predicted towards *Erwiniaceae* and mutualism of *Staphylococcaceae* members with *K. pneumoniae* need further study utilizing the ISS strains.

At the genus level, we observed that *Pantoea* genus typically derives the most benefit in the community. On looking at the pairwise interactions, we observed that amongst other *Enterobacteriaceae, K. pneumoniae* provides metabolic support to many of its coexisting species, notably those from the *Pantoea* genus. The members of the genus *Pantoea* were primarily considered as plant pathogens, but subsequently, they have been isolated from many aquatic and terrestrial environments, including ISS [8] as well as in association with insects, animals and humans [45–49]. During this study [8], the metagenomic sequences of the opportunistic human pathogens associated with *Pantoea* genus were *P. agglomerans, P. conspicua, P. brenneri, P. ananatis* and *P. dispersa,* whereas the plant pathogenic *Pantoea* species were not observed. The competitive metabolomic properties predicted during this study by *K. pneumoniae* with *Pantoea* members (Fig. 6A) might be due to the assimilation of similar compounds for sustaining their growth. Detailed phenotypic metabolic profiles of these microbes are needed to confirm the competition and amensalism predicted in this study.

Finally, from the constraint-based analyses, many amensal and parasitic interactions were noticed. This is corroborated by earlier findings that *K. pneumoniae* can inhibit fungal conidia germination and hyphal growth, as well as biofilm formation of *Aspergillus* species [50]. Recent reports documented that *K. pneumoniae* shifted to a pathogenic state, potentially leading to septic infections when cooccurred with *A. fumigatus* in immunocompromised individuals [50]. In addition, this study shows that *K. pneumoniae* cells prevented germination of conidia and hyphal development of the fungi. It has been further shown that *K. pneumoniae* bacterial cells induced the fungal cell wall stress response mechanisms and suppressed the filamentous growth of fungi [50]. The simple in silico metabolic model of this study predicted the antagonistic (parasitic) metabolic interaction between *K. pneumoniae* and *A. niger* (Fig. 6B), which further enabled to validate parasitism in vivo, using the strains isolated from the ISS. However, this experimental evidence might not be enough to fully prove the metabolic prediction. Additional positive and negative controls are necessary, which would further improve the evidence of antagonistic metabolic interaction predicted during this study. Furthermore, quantitative measurements of *K. pneumoniae* and *Aspergillus* growth are needed to validate the computational prediction of this study and warrants further study.

Our study does have some limitations. First, the metabolic models used in the study are automated reconstructions, which despite gap-filling, could potentially contain gaps and blocked reactions and need to be curated [51]. Nevertheless, such automated reconstructions are being widely used in many studies as they serve as useful predictive tools and representations of the metabolism of microorganisms [52]. Secondly, wherever it is applicable, genomes generated from the cultured ISS microorganisms were utilized. Conversely, when strains were not isolated from the ISS environment, and thus, genomes were not available, the reference genomes of the corresponding type strains were used. However, reference genomes provide a useful perspective of an organism's metabolic capabilities and have also been used in many other studies that incorporate metabolic models [53, 54]. In the absence of exact estimates of environmental metabolites, we posited that the environment had at least the minimal set of metabolites necessary for a given organism to survive, and also included additional cofactors and coenzymes. We assumed that each microorganism is capable of minimal independent growth and thus calculated the minimal medium required to support survival. It is possible that some of the interactions remain conserved, in richer media, although others may disappear, depending on the inherent metabolic capabilities of the organisms.

The graph-based approach provides a somewhat static snapshot of the metabolic interactions happening between the organisms. Indeed, the graph-theoretic approach does not account for differential importance of reactions, or for example, the increase in growth rate, that may result from potential interactions. This is captured by the complementary constraint-based modeling approaches that were employed, and together, we believe, they provide a more complete picture of the possible interactions between the microbes. As previously highlighted in the 'Methods' section as well, there have been previous reports wherein a higher MSI does

point towards a possible higher biomass in the community. As reported for *Candida albicans,* in addition to the genome-scale metabolic model, refining the model using phenotypic microarray and other wet-lab confirmation are needed [55]. Yet, it is highly useful and offers valuable insights into the potential microbial interactions in the community [30, 56] and well complements the constraint-based methods. Of course, it is important to emphasize that our computational methodology studies microbes through a metabolic lens only, and in reality, other interactions may be plausible. Nevertheless, metabolic interactions have been previously shown [21] to be important drivers of community structure and microbial interactions. Importantly, this study offers a first glimpse into the metabolic interactions of the ISS microbiome, upon which several hypotheses can be formulated for future experimental design.

Conclusion

In summary, our analyses show the key role played by *Klebsiella* and other *Enterobacteriaceae* in mediating the metabolic interactions taking place between microorganisms in the ISS. Metabolic modeling, through a combination of graph-theoretic approaches and steady-state constraint-based modeling, paints a more comprehensive picture of possible microbial interactions, which are as yet inscrutable to this extent by experimental approaches. Our results point towards key dependencies of microorganisms in various locations on the ISS and can pave the way for possible interventions that may rely on targeted disinfection of surfaces aboard the ISS. Our approach also underscores the importance of complementary modeling approaches in dissecting a fairly complex microbiome and understanding various possible interactions. Our methodology is fairly generic and can be readily extended to predict microbial interactions in other interesting milieu and generate testable hypotheses for wet lab experiments, as we have demonstrated in this study with *Klebsiella and Aspergillus* species.

Abbreviations

BSL – 2: Biosafety Level 2; CSI: Community Support Index; ISS: International Space Station; MSI: Metabolic Support Index.

Supplementary Information

The online version contains supplementary material available at https://doi.org/10.1186/s40168-022-01279-y.

Additional file 1: Supplementary Methods M1. Genome-scale metabolic reconstruction and modeling.

Additional file 2: Supplementary Figure S1. BSL-2 pathogens. The word cloud shows the dominant and persistent BSL-2 pathogens at each location in each flight.

Additional file 3: Supplementary Figure S2. Extent of metabolic benefit conferred by an individual microorganism to its coexisting microorganisms. The heatmap depicts the range of Community Support Indices ($CSI_{A \to \tilde{A}}$) that indicate the metabolic support rendered by an individual microorganism to its coexisting microorganisms, by virtue of it being in that location. On the X-axis is the list of microorganisms in consideration, and on the Y-axis is the flight number and the concerned location number. A darker blue tile indicates the microorganism is highly beneficial.

Additional file 4: Supplementary Figure S3. Microbial association networks depicting the metabolic dependencies of *E. coli* and its coexisting microorganisms on each other, during Flight 3. Cytoscape was used to construct and visualize these networks across all locations during Flight 3 (F3). The nodes are labelled with microorganisms that co-inhabit that location with *E. coli*. The directed edges are directed from the metabolically supportive microorganism to the metabolically dependent microorganism. The color of these directed edges are mapped to the Metabolic Support Indices (MSI), represented as percentages, such that the gradient from light blue to dark blue represents an increasing MSI.

Additional file 5: Supplementary Figure S4. Microbial association networks depicting the metabolic dependencies of *S. enterica* and its coexisting microorganisms on each other, during Flight 3. Cytoscape was used to construct and visualize these networks across all locations during Flight 3 (F3). The nodes are labelled with microorganisms that co-inhabit that location with *S. enterica*. The directed edges are directed from the metabolically supportive microorganism to the metabolically dependent microorganism. The color of these directed edges is mapped to the Metabolic Support Indices (MSI), represented as percentages, such that the gradient from light blue to dark blue represents an increasing MSI.

Additional file 6: Supplementary Figure S5. Morphological architecture of *A. fumigatus* in the presence and absence of *K. pneumoniae*. (A) *A. fumigatus* grown under normal gravity, (B) Both bacteria and fungus grown under normal gravity, (C) *A. fumigatus* grown under simulated gravity, and (D) Both bacteria and fungus grown under simulated gravity. These pictures are representative micrographs of hundreds of SEM images.

Additional file 7: Supplementary Figure S6. Polymeric filamentous structures of *A. fumigatus* when co-cultured with *K. pneumoniae* under simulated microgravity. (A) *A. fumigatus* grown under normal gravity, (B) Both bacteria and fungus grown under normal gravity, (C) *A. fumigatus* grown under simulated gravity, and (D) Both bacteria and fungus grown under simulated gravity. White arrows shown in A and C were speculated to be the polymeric filamentous structures that might enable the fungus to form biofilm. However, when *K. pneumoniae* cells co-cultured with *A. fumigatus* (B and D) polymeric filamentous structures were not noticed. Yellow arrows were speculated to be the degraded fungal products by *K. pneumoniae* cells. When both bacteria and fungus grown under normal (B) or simulated gravity (D), the polymeric substances are not observed. However as shown in panel D, these structures are virtually not present. These pictures are the representative micrographs of hundreds of SEM images.

Additional file 8: Supplementary Table S1. RefSeq and GenBank Accession identification numbers for the microorganisms used in this study. **Supplementary Table S2.** Details of genome-scale metabolic network reconstructions. **Supplementary Table S3.** List of seed metabolites used in the analyses. **Supplementary Table S4.** Relative abundances of microorganisms in the flight-locations considered. **Supplementary Table S5.** Metabolic benefit provided by an individual microorganism to the rest of the community. **Supplementary Table S6.** Metabolic benefit provided by each family to the rest of the community. **Supplementary Table S7.** Metabolic support provided to an individual microorganism by the rest of the community. **Supplementary Table S8.** Metabolic support provided to an individual microorganism by another microorganism in the community. **Supplementary Table S9.** Nature of interactions as predicted by the constraint-based analyses.

Authors' contributions

KV and KR were involved in early organization, study design, and planning of the project, and providing direct feedback to all authors throughout the project and during write-up of the manuscript. RKK and SB wrote the manuscript. RKK generated all figures in the manuscript, processed the data and constructed metabolic models, and performed the MSI-based analyses. SB performed the constraint-based analysis and determined the nature of interactions. NKS was involved in study design, helped interpret and write the manuscript, and generated metagenome data and bioinformatic analysis. CWP carried out the microscopy and confirmed the parasitic aspect of *Klebsiella* and *Aspergillus* species. The authors reviewed, read and approved the final manuscript.

Availability of data and materials

The metagenomic sequence data used in this study can be found under NCBI Short Read Archive (SRA) under the bio-project number PRJNA438545 and GeneLab dataset GLDS-69 (https://genelab-data.ndc.nasa.gov/genelab/accession/GLDS-69/). The genome-scale metabolic network reconstructions, the seed metabolites, and the codes used in this study, have been provided at https://github.com/RamanLab/Metabolic-Modelling-of-the-ISS-Microbiome.

Declarations

Ethics approval and consent to participate

No human subjects were analyzed and only environmental samples were collected.

Consent for publication

All authors participated in this study and given their consent for publishing the results.

Competing interests

The authors declare that they have no competing interests.

Author details

[1]Robert Bosch Centre for Data Science and Artificial Intelligence (RBCDSAI), Indian Institute of Technology Madras, Chennai 600 036, India. [2]Center for Integrative Biology and Systems mEdicine (IBSE), Indian Institute of Technology Madras, Chennai 600 036, India. [3]NASA Jet Propulsion Laboratory, California Institute of Technology, Pasadena, M/S 89-2, 4800 Oak Grove Dr, Pasadena, CA CA 91109, USA. [4]Department of Biotechnology, Bhupat and Jyoti Mehta School of Biosciences, Indian Institute of Technology Madras, Chennai 600 036, India.

References

1. Shafquat A, Joice R, Simmons SL, Huttenhower C. Functional and phylogenetic assembly of microbial communities in the human microbiome. Trends Microbiol. 2014;22:261–6.
2. Vandenkoornhuyse P, Quaiser A, Duhamel M, le Van A, Dufresne A. The importance of the microbiome of the plant holobiont. New Phytol. 2015;206:1196–206.
3. Konopka A. What is microbial community ecology. ISME J. 2009;3:1223–30.
4. National Academies of Sciences, Eengineering, and Medicine. Microbiomes of the Built Environment: A Research Agenda for Indoor Microbiology, Human Health, and Buildings. Washington, DC: The National Academies Press; 2017.
5. Bijlani S, Singh NK, Eedara VVR, Podile AR, Mason CE, Wang CCC, et al. *Methylobacterium ajmalii* sp. nov., isolated from the international space station. Front Microbiol. 2021;12:534.
6. Singh NK, Wood JM, Mhatre SS, Venkateswaran K. Correction to: metagenome to phenome approach enables isolation and genomics characterization of *Kalamiella piersonii* gen. nov., sp. nov. from the International Space Station. Appl Microbiol Biotechnol. 2019;103:6851–2.
7. Checinska Sielaff A, Kumar RM, Pal D, Mayilraj S, Venkateswaran K. *Solibacillus kalamii* sp. nov., isolated from a high-efficiency particulate arrestance filter system used in the International Space Station. Int J Syst Evol Microbiol. 2017;67:896–901.
8. Checinska Sielaff A, Urbaniak C, Mohan GBM, Stepanov VG, Tran Q, Wood JM, et al. Characterization of the total and viable bacterial and fungal communities associated with the International Space Station surfaces. Microbiome. 2019;7:1–21.
9. Avila-Herrera A, Thissen J, Urbaniak C, Be NA, Smith DJ, Karouia F, et al. Crewmember microbiome may influence microbial composition of ISS habitable surfaces. PLoS One. 2020;15:e0231838.
10. Castro VA, Thrasher AN, Healy M, Ott CM, Pierson DL. Microbial characterization during the early habitation of the international space station. Microb Ecol. 2004;47:119–26.
11. Venkateswaran K, Vaishampayan P, Cisneros J, Pierson DL, Rogers SO, Perry J. International Space Station environmental microbiome - microbial inventories of ISS filter debris. Appl Microbiol Biotechnol. 2014;98:6453–66.
12. Be NA, Avila-Herrera A, Allen JE, Singh N, Checinska Sielaff A, Jaing C, et al. Whole metagenome profiles of particulates collected from the International Space Station. Microbiome. 2017;5:81.
13. Checinska A, Probst AJ, Vaishampayan P, White JR, Kumar D, Stepanov VG, et al. Microbiomes of the dust particles collected from the International Space Station and Spacecraft Assembly Facilities. Microbiome. 2015;3:50.
14. Lang JM, Coil DA, Neches RY, Brown WE, Cavalier D, Severance M, et al. Correction: a microbial survey of the International Space Station (ISS). PeerJ. 2018;5:e4029/correction-1.
15. Singh NK, Wood JM, Karouia F, Venkateswaran K. Correction to: Succession and persistence of microbial communities and antimicrobial resistance genes associated with International Space Station environmental surfaces. Microbiome. 2018;6:204. https://doi.org/10.1186/s40168-018-0585-2.
16. Wyres KL, Lam MMC, Holt KE. Population genomics of *Klebsiella pneumoniae*. Nat Rev Microbiol. 2020;18:344–59.
17. Clegg S, Murphy CN. Epidemiology and Virulence of *Klebsiella pneumoniae*. In: Urinary Tract Infections. Washington, DC: ASM Press; 2016. p. 435–57.
18. Pendleton JN, Gorman SP, Gilmore BF. Clinical relevance of the ESKAPE pathogens. Expert Rev Anti-Infect Ther. 2013;11:297–308.
19. Podschun R, Ullmann U, *Klebsiella* spp. as nosocomial pathogens: epidemiology, taxonomy, typing methods, and pathogenicity factors. Clin Microbiol Rev. 1998;11:589–603.
20. Bengoechea JA, Sa PJ. *Klebsiella pneumoniae* infection biology: living to counteract host defences. FEMS Microbiol Rev. 2019;43:123–44.
21. Ponomarova O, Patil KR. Metabolic interactions in microbial communities: untangling the Gordian knot. Curr Opin Microbiol. 2015;27:37–44.
22. Shoaie S, Karlsson F, Mardinoglu A, Nookaew I, Bordel S, Nielsen J. Understanding the interactions between bacteria in the human gut through metabolic modeling. Sci Rep. 2013;3:1–10.
23. Zelezniak A, Andrejev S, Ponomarova O, Mende DR, Bork P, Patil KR. Metabolic dependencies drive species co-occurrence in diverse microbial communities. Proc Natl Acad Sci U S A. 2015;112:6449–54.
24. Thommes M, Wang T, Zhao Q, Paschalidis IC, Segrè D. Designing metabolic division of labor in microbial communities. mSystems. 2019;4:263–81.
25. McCloskey D, Palsson BØ, Feist AM. Basic and applied uses of genome-scale metabolic network reconstructions of *Escherichia coli*. Mol Syst Biol. 2013;9:661.
26. Thiele I, Palsson B. A protocol for generating a high-quality genome-scale metabolic reconstruction. Nat Protoc. 2010;5:93–121.

27. Kumar M, Ji B, Zengler K, Nielsen J. Modeling approaches for studying the microbiome. Nat Microbiol. 2019;4:1253–67.
28. Ravikrishnan A, Raman K. Systems-level modeling of microbial communities. Boca Raton: CRC Press; 2018.
29. Ravikrishnan A, Nasre M, Raman K. Enumerating all possible biosynthetic pathways in metabolic networks. Sci Rep. 2018;8:9932.
30. Ravikrishnan A, Blank LM, Srivastava S, Raman K. Investigating metabolic interactions in a microbial co-culture through integrated modeling and experiments. Comput Struct Biotechnol J. 2020;18:1249–58.
31. Chan SHJ, Simons MN, Maranas CD. SteadyCom: predicting microbial abundances while ensuring community stability. PLoS Comput Biol. 2017;13:e1005539.
32. Vaishampayan P, Probst AJ, la Duc MT, Bargoma E, Benardini JN, Andersen GL, et al. New perspectives on viable microbial communities in low-biomass cleanroom environments. ISME J. 2013;7:312–24.
33. Arkin AP, Cottingham RW, Henry CS, Harris NL, Stevens RL, Maslov S, et al. KBase: The United States department of energy systems biology knowledgebase. Nat Biotechnol. 2018;36:566–9.
34. Henry CS, Dejongh M, Best AA, Frybarger PM, Linsay B, Stevens RL. High-throughput generation, optimization and analysis of genome-scale metabolic models. Nat Biotechnol. 2010;28:977–82.
35. Ebrahim A, Lerman JA, Palsson BO, Hyduke DR. COBRApy: constraints-based reconstruction and analysis for Python. BMC Syst Biol. 2013;7:74.
36. Shannon P, Markiel A, Ozier O, Baliga NS, Wang JT, Ramage D, et al. Cytoscape: a software environment for integrated models of biomolecular interaction networks. Genome Res. 2003;13:2498–504.
37. Großkopf T, Soyer OS. Synthetic microbial communities. Curr Opin Microbiol. 2014;18:72–7.
38. Norsigian CJ, Attia H, Szubin R, Yassin AS, Palsson BØ, Aziz RK, et al. Comparative genome-scale metabolic modeling of metallo-beta-lactamase–producing multidrug-resistant *Klebsiella pneumoniae* clinical isolates. Front Cell Infect Microbiol. 2019;9:161.
39. Heinken A, Thiele I. Anoxic conditions promote species-specific mutualism between gut microbes In Silico. Appl Environ Microbiol. 2015;81:4049–61.
40. Orsini SS, Lewis AM, Rice KC. Investigation of simulated microgravity effects on streptococcus mutans physiology and global gene expression. NPJ Microgravity. 2017;3:4.
41. Venturelli OS, Carr A, Fisher G, Hsu RH, Lau R, Bowen BP, et al. Deciphering microbial interactions in synthetic human gut microbiome communities. Mol Syst Biol. 2018;14:e8157.
42. Basaran P. Inhibition effect of belzalkonium chloride treatment on growth of common food contaminating fungal species. J Food Sci Technol. 2011;48:515–9.
43. Sushenko N, Gans J, Arambula C, Singh N, Venkateswaran K, Moser D. Disinfectant resistance of *Klebsiella pneumoniae* strains isolated from the International Space Station. In: 20th Annual Meeting of the American Society for the Gravitational and Space Research; 2020.
44. Soliman H, Elsayed A, Dyaa A. Antimicrobial activity of silver nanoparticles biosynthesised by *Rhodotorula* sp. strain ATL72. Egypt J Basic Appl Sci. 2018;5:228–33.
45. Muraschi TF, Friend M, Bolles D. *Erwinia*-like microorganisms isolated from animal and human hosts. Appl Microbiol. 1965;13:128.
46. Ewing WH, Fife MA. *Enterobacter agglomerans* (Beijerinck) comb. nov. (the Herbicola-Lathyri Bacteria). Int J Syst Evol Microbiol. 1972;22:4–11.
47. Brady C, Cleenwerck I, Venter S, Vancanneyt M, Swings J, Coutinho T. Phylogeny and identification of *Pantoea* species associated with plants, humans and the natural environment based on multilocus sequence analysis (MLSA). Syst Appl Microbiol. 2008;31:447–60.
48. Völksch B, Thon S, Jacobsen ID, Gube M. Polyphasic study of plant- and clinic-associated *Pantoea agglomerans* strains reveals indistinguishable virulence potential. Infect Genet Evol. 2009;9:1381–91.
49. Nadarasah G, Stavrinides J. Quantitative evaluation of the host-colonizing capabilities of the enteric bacterium *Pantoea* using plant and insect hosts. Microbiology. 2014;160:602–15.
50. Nogueira MF, Pereira L, Jenull S, Kuchler K, Lion T. *Klebsiella pneumoniae* prevents spore germination and hyphal development of *Aspergillus* species. Sci Rep. 2019;9:1–15.
51. Ravikrishnan A, Raman K. Critical assessment of genome-scale metabolic networks: the need for a unified standard. Brief Bioinform. 2015;16:1057–68.
52. Gu C, Kim GB, Kim WJ, Kim HU, Lee SY. Current status and applications of genome-scale metabolic models. Genome Biol. 2019;20:1–18.
53. Machado D, Maistrenko OM, Andrejev S, Kim Y, Bork P, Patil KR, et al. Polarization of microbial communities between competitive and cooperative metabolism. Nat Ecol Evol. 2021;5:195–203.
54. Garza DR, van Verk MC, Huynen MA, Dutilh BE. Towards predicting the environmental metabolome from metagenomics with a mechanistic model. Nat Microbiol. 2018;3:456–60.
55. Mirhakkak MH, Schäuble S, Klassert TE, Brunke S, Brandt P, Loos D, et al. Metabolic modeling predicts specific gut bacteria as key determinants for *Candida albicans* colonization levels. ISME J. 2020;15:1257–70.
56. Chng KR, Ghosh TS, Tan YH, Nandi T, Lee IR, Ng AHQ, et al. Metagenome-wide association analysis identifies microbial determinants of post-antibiotic ecological recovery in the gut. Nat Ecol Evol. 2020;4:1256–67.

Publisher's Note